Modeling of Notch Tensile Behavior of Martensitic Steels

M.M. Megahed, N.M. Abd-Allah, and A.M. Eleiche

(Submitted 2 February 2001)

Notch tensile tests have been carried out on six grades of a high-strength martensitic steel at different hardness levels to investigate the effects of stress triaxiality at the net section and uniaxial tensile properties on fracture behavior. Cylindrical V-notched specimens were used in these tests with the notch-root radius, ρ, ranging from 0.03-1.4 mm, and with the value of the net-to-gross diameter ratio being 0.6. The notch strength ratio (NSR) was found to attain its maximum value at ρ = 0.38 mm. The test results were used successfully for screening the fracture toughness behavior of the martensitic steel by extrapolating the corresponding ρ-NSR curve to ρ = 0.0. Further, finite element computation of the average stress triaxiality factor ($\overline{\eta}$) enabled the development of a model more accurate than that reported in the literature for estimating NSR for a ductile material as a function of $\overline{\eta}$ and its uniaxial tensile properties.

Keywords finite element modeling, martensitic steel, notch-root radius, notch-strength ratio, stress-triaxiality factor, v-notched tensile specimens

1. Introduction

The introduction of a notch in an engineering component or a test specimen results in stress concentration, a state of triaxial stresses, and reduced ductility. The notch tensile test has been frequently performed using notched cylindrical specimens to evaluate the effects of stress triaxiality and uniaxial tensile properties on notch strength ratio (NSR). This ratio is defined as[1]:

$$NSR = \frac{S_{un}}{S_u} \qquad \text{(Eq 1)}$$

where S_{un} and S_u are the ultimate tensile strengths (UTS) in notched and smooth specimens, respectively. In notch-strengthened condition, the value of NSR is more than unity. On the other hand, in notch-weakened condition, the value of NSR is less than unity. From previous investigations,[2-5] three main conclusions were obtained:

1) For a notch radius greater than a certain value determined by material ductility, the NSR decreases with increasing notch radius.
2) The NSR increases with increasing notch depth up to approximately one-half of the net-to-gross diameter.
3) For low-strength materials, the NSR can be estimated as a function of the average stress triaxiality factor at the net section, $\overline{\eta}$, and the ratio of local to total elongation (δ_L/δ_T) in the uniaxial tensile engineering stress-strain curve, where δ_L and δ_T are measured from maximum load, and initial loading, respectively, to fracture. The stress triaxiality factor (η) has been defined as the ratio between three times the mean hydrostatic stress ($3\sigma_m$), and the Von-Mises equivalent stress (σ_{eq})[6]:

$$\eta = \frac{\sqrt{2}(\sigma_1 + \sigma_2 + \sigma_3)}{\sqrt{(\sigma_1 - \sigma_2)^2 + (\sigma_2 - \sigma_3)^2 + (\sigma_3 - \sigma_1)^2}} = \frac{3\sigma_m}{\sigma_{eq}} \qquad \text{(Eq 2)}$$

where

- σ_m = mean stress = $(\sigma_1 + \sigma_2 + \sigma_3)/3$;
- $\sigma_1, \sigma_2, \sigma_3$ = longitudinal, tangential, and radial principal stresses, respectively; and
- σ_{eq} = effective stress = $\sqrt{[(\sigma_1 - \sigma_2)^2 + (\sigma_2 - \sigma_3)^2 + (\sigma_3 - \sigma_1)^2]}/\sqrt{2}$.

Further, many investigations have been devoted to evaluating the plane strain fracture toughness behavior from cylindrical bar notch-tensile measurements, but there is no unique estimation of K_{IC} behavior using such specimens.[6,7] In the current study, notch tensile test results of high strength steels have been used for screening the corresponding fracture toughness behavior and for the accurate modeling of NSR of the notched tensile specimens of the steel in terms of stress triaxiality and tensile properties.

2. Experimental Procedure

2.1 Material

The material selected for the current study is used in manufacturing the main parts of machine-gun weapons. A grade of medium alloy steel (30XH2M∅A; Russian specs GOST 4543.57) supplied in the forged condition, whose chemical composition is listed in Table 1, was used. After being rough machined longitudinally from the delivered stock, specimens were heat treated by austenizing at 850 °C for 15 min and then oil quenched. To avoid any aging, immediately thereafter the specimens were tempered for 2 h at six different temperatures: 650, 630, 600, 540, 400, and 200 °C, and then air-cooled to

M.M. Megahed, Mechanical Design and Production Department, Faculty of Engineering, Cairo University, Egypt; **N.M. Abd-Allah,** Technical Departments, Maadi Company for Engineering Industry, Cairo, Egypt; **A.M. Eleiche,** Mechanical Engineering Department, King Fahd University of Petroleum and Minerals, Dhahran, Saudi Arabia. Contact e-mail: eleichea@kfupm.edu.sa.

Table 1 Chemical Composition, wt.%, of the Investigated Steel 30XH2MØA; GOST 4543.57

C	Mn	Si	P	S	Cr	Ni	Mo	Cu	V
0.3	0.46	0.31	0.021	0.011	0.79	2.07	0.42	0.07	0.26

Table 2 Uniaxial Tensile Properties and Fracture Toughness K_{IC} and J_{IC} Properties of 30XH2MØA Martensitic Steel at Six Material Conditions[8]

Material Designation	σ_{ys}, Mpa	S_u, Mpa	RA, %	σ_f, MPa	δ_I/δ_T	K_{IC}, MPa $\sqrt{m}$	J_{IC}, KJ/m^2
A1 (270 HB)	857	906	63	1583	0.65	…	139.7
A2 (305 HB)	1001	1042	60	1729	0.62	…	174.5
A3 (340 HB)	1110	1151	58	1875	0.61	…	151.0
A4 (370 HB)	1185	1252	55	1980	0.67	…	90.3
A5 (420 HB)	1370	1470	51	2221	0.71	87.95	…
A6 (475 HB)	1485	1644	45	2410	0.64	91.55	…

room temperature (RT). This treatment yielded six high-strength martensitic steel grades with hardness values of 270, 305, 340, 370, 420, and 475 Brinell hardness (HB), designated hereafter by A1, A2, A3, A4, A5, and A6, respectively. The uniaxial tensile properties and fracture toughness K_{IC} and J_{IC} properties of the six steel grades were determined experimentally,[8] and are listed in Table 2.

2.2 Specimens

Figure 1 depicts the notched tensile specimen geometry used in the current study. The specimens were semifinished by machining after carrying out the aforementioned heat treatment operations. All specimens were then ground to the given dimensions, with the V-notches being finally machined using honed carbide form tools. The net diameter (d) and the value of the net-to-gross diameter ratio (d/D) are 6 mm and 0.6, respectively. The notch effect was varied by employing five different notch radii (ρ): 0.03, 0.25, 0.38, 0.5, and 1.4 mm. For each steel grade, two specimens were used for each value of the notch radius. As inspected using an optical comparator, the maximum run-out at the notched section and on the thread root diameter was found to be less than 0.05 mm.[9]

3. Results and Discussion

3.1 Notch Tension Behavior

Notch tensile tests were carried out on the six steel grades at RT. Table 3 lists the NSR (= S_{un}/S_u), and the percent reduction of notched-net-sectional area (RA_n%). Figure 2 depicts the variation of S_{un} with notch-root radius (ρ), while Fig. 3 shows the variation of NSR with ρ. All tested grades exhibit notch strengthening. Further, the figures indicate that both S_{un} and NSR attain their maximum values at ρ = 0.38 mm. By extrapolating the NSR-ρ curves for grades A1, A2, A3, and A4 to ρ ≈ 0.0, notch strengthening can be expected for relatively small specimen sizes with fatigue cracks. For the other two

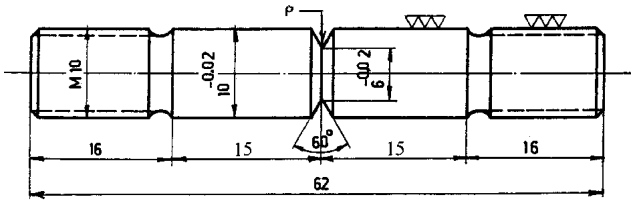

Fig. 1 Configuration of the notched tensile test specimen

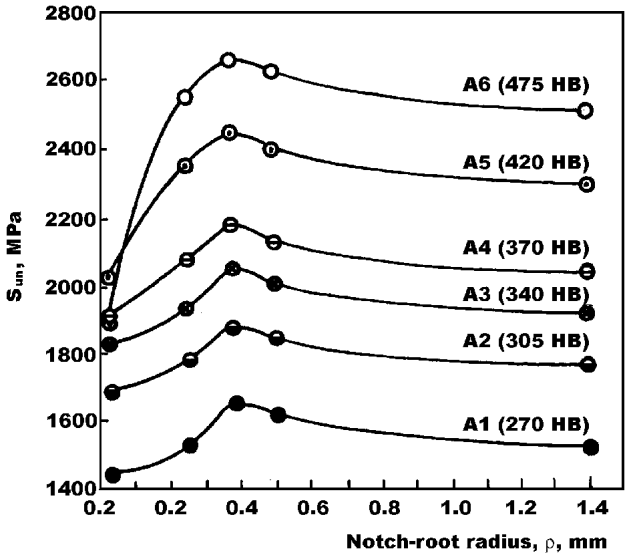

Fig. 2 Variation of UTS in notched specimen, S_{un}, with notch-root radius, ρ

grades, notch weakening can be expected for the A6 grade and is possible for the A5 grade using specimens of relatively small sizes with fatigue cracks.

Figure 4 depicts the variation of S_{un} with hardness at different notch-root radii. For notch radius ρ ≥ 0.25 mm, the S_{un} increases with the increase of material hardness. Further, the notch radius 0.38 mm represents the optimum notch-sharpness to attain the maximum S_{un} value within the hardness range 270-475 HB. Consequently, the maximum S_{un} value in notched specimens of this steel is obtained with notch radius 0.38 mm and hardness 475 HB. On the other hand, at ρ = 0.03 mm, S_{un} attains its peak value at 420 HB; thereafter, it begins to decrease sharply with increase in hardness. This indicates the predictability of material notch sensitivity at hardness values higher than 420 HB and in the presence of fatigue cracks, using specimens of relatively small sizes.

Figure 5 shows the variation of NSR with hardness at different notch radii. For notch radii exceeding 0.25 mm, the NSR value is almost constant within the considered hardness range 270-475 HB. On the other hand, at ρ = 0.03 mm, NSR is almost constant within hardness range 270-340 HB. Above 420 HB, it begins to decrease sharply with hardness. Consequently, a notch-weakening condition is predicted within the hardness range 420-475 HB for fatigue-cracked specimens of relatively small sizes.

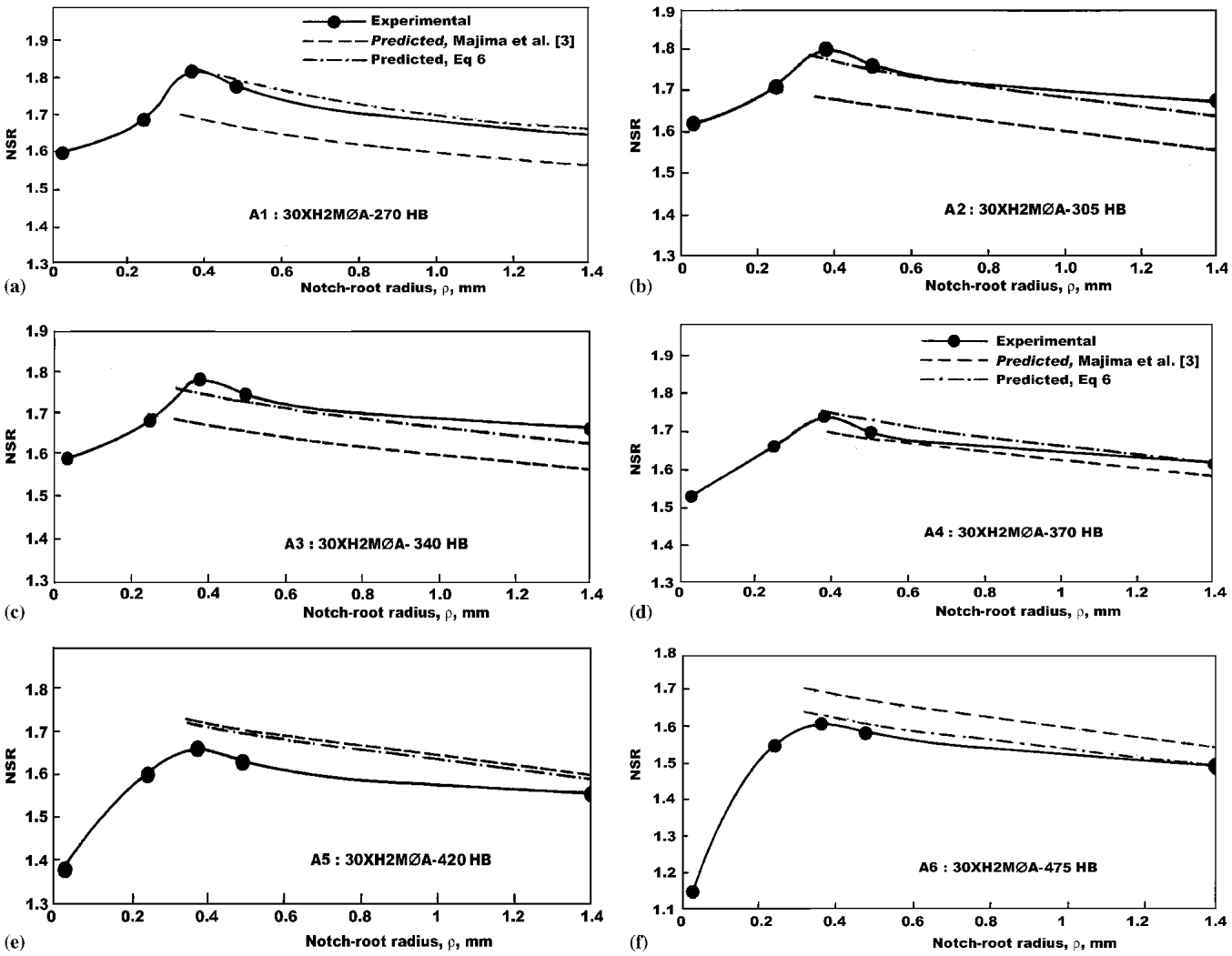

Fig. 3 Variation of NSR with ρ for all investigated steel grades

Table 3 Notch Tension Test Results

Material Designation	Notch-Root Radius, mm									
	0.03		0.25		0.38		0.5		1.4	
	NSR (a)	RA_n%	NSR	RA_n%	NSR	RA_n%	NSR	RA_n%	NSR	RA_n%
A1 (270 HB)	1.60	20.0	1.69	20.5	1.82	21.4	1.78	22.9	1.66	29.4
A2 (305 HB)	1.62	15.2	1.71	16.1	1.80	16.5	1.76	18.6	1.67	24.1
A3 (340 HB)	1.59	12.8	1.68	13.3	1.78	13.7	1.74	15.5	1.65	21.6
A4 (370 HB)	1.53	10.5	1.66	10.6	1.74	10.9	1.70	12.7	1.62	18.5
A5 (420 HB)	1.38	8.3	1.60	8.7	1.66	9.2	1.63	11.1	1.55	16.5
A6 (475 HB)	1.15	5.9	1.55	6.8	1.61	7.3	1.59	9.9	1.51	15.3

(a) NSR, notch strength ratio; RA_n%, percent reduction of notched-net-sectional area

The notch-weakening predictability of 30XH2M∅A steel within hardness zone 420-475 HB, as discussed above, corresponds well with the measured fracture toughness behavior of the six steel grades as depicted in Table 2, where K_{IC} and J_{IC} were determined according to ASTM E399[10] and E813[11] test methods, using Single Edge Notched Bend (SENB) specimens of thickness B = 12.5 mm. Thus, notch tension tests may be used for screening fracture toughness behavior of high strength ductile steels.

3.2 Finite Element Computation of $\bar{\eta}$

The average stress triaxiality factor ($\bar{\eta}$) across the notched section has been computed using finite element (FE) analysis.

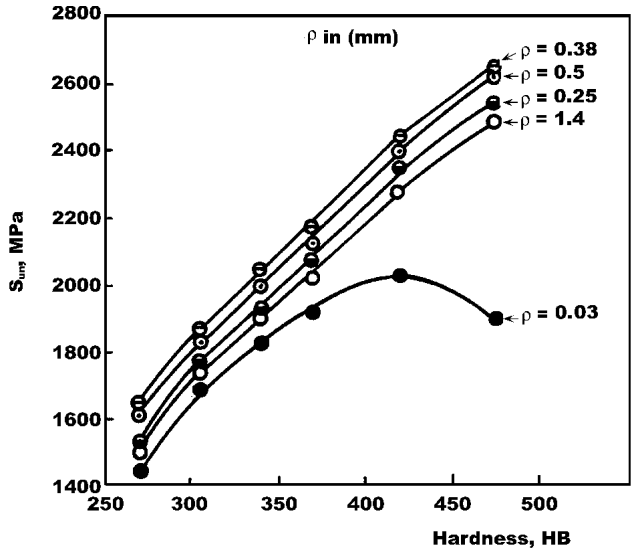

Fig. 4 Variation of UTS in notched specimens, S_{un}, with hardness at different notch radii

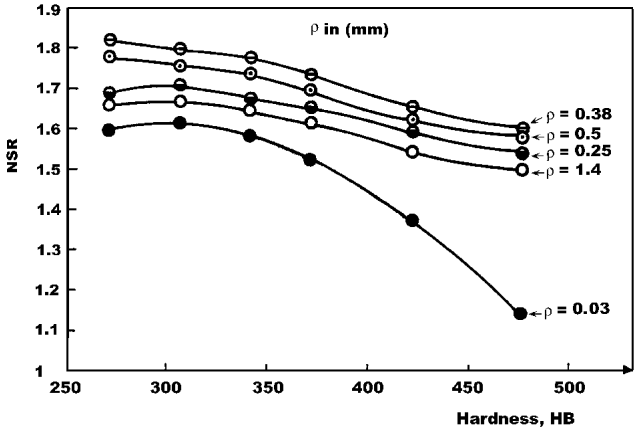

Fig. 5 Variation of NSR with hardness at different notch radii

This enabled modeling of the observed behavior of the steel in notched tensile testing. Figure 6(a) depicts the FE idealization of the round-notched specimen with notch radius of 0.25 mm. Due to symmetry, only one quadrant of the specimen is considered. The meshing consists of 8-noded quadrilateral (axisymmetric) elements, and 6-noded triangular (axisymmetric) elements. A high degree of mesh refinement (smallest element size = 0.005 mm^2) is considered to capture the rapid change in stress gradient at the notch root and across the notch net section. The boundary conditions in the FE idealization of the notched specimen are shown in Fig. 6(b).

The accuracy of the model has been checked by comparing the FE-computation results of the elastic theoretical stress concentration factor (K_t) at the notch root for the five notch geometries with the corresponding analytically determined values. Figure 7(a) depicts the distribution of the principal stresses and triaxiality factor, η, across the notched section with ρ = 0.25 mm in the elastic material state. The computed K_t is 3.63, which differs by less than 2% from the analytically calculated value of 3.70.[12] Consequently, the same idealization was

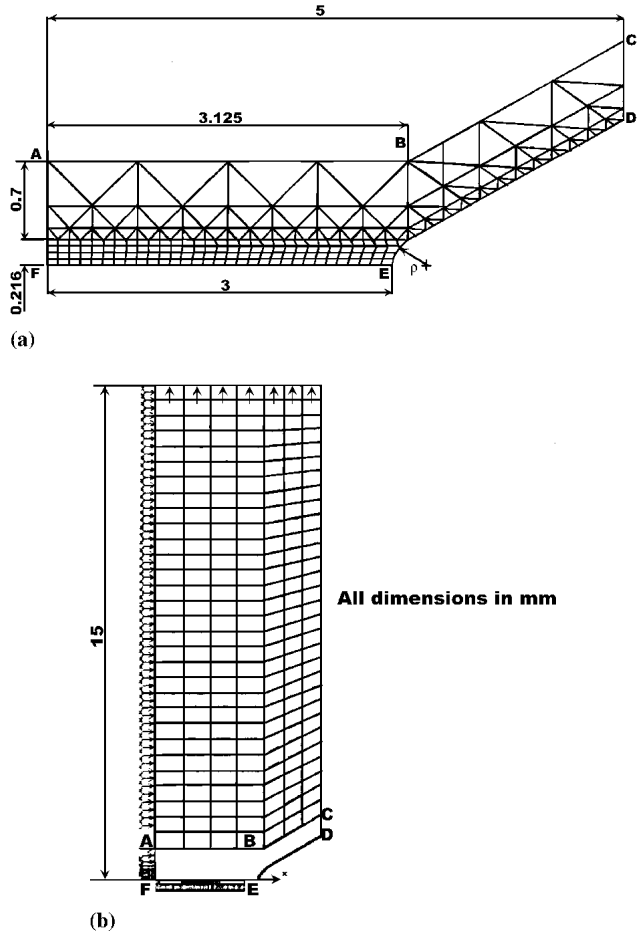

Fig. 6 Typical example of: **(a)** FE idealization, and **(b)** boundary conditions, for the notched tensile specimen

used, as shown in Fig. 7(b), to compute the principal stresses and η for an elasto-plastic material model of tangent modulus E_t (= dσ/dε) taken as 0.01E. Figure 8(a) and (b) shows the variation of η(r) for the elastic and elastic-plastic material states, respectively, for different values of ρ. The figures indicate that η acquires its maximum value at the center of the blunt notch (ρ = 1.4 mm). Further, the increase in notch sharpness is associated with the increase in the values of η across the notched section and a shift in the location of the maximum value of η from the center for the bluntly notched specimens towards the notch tip for the sharply notched specimens. Consequently, associated with increasing to decreasing NSR as the notch sharpness increases (Fig. 3) is a shift in the location of fracture initiation from the center for bluntly notched specimens to the notch tip for sharply notched specimens.

Figure 7(b) indicates that at a point of distance r from the center of the notched section, the value of the triaxiality factor is η(r). Thus, the average computed $\bar{\eta}$ across the notched section is obtained as follows:

$$\bar{\eta} = \frac{\int_o^{d/2} \eta(r) 2\pi r dr}{\pi (d/2)^2} = \frac{8}{d^2} \int_o^{d/2} r \cdot \eta(r) dr \qquad \text{(Eq 3)}$$

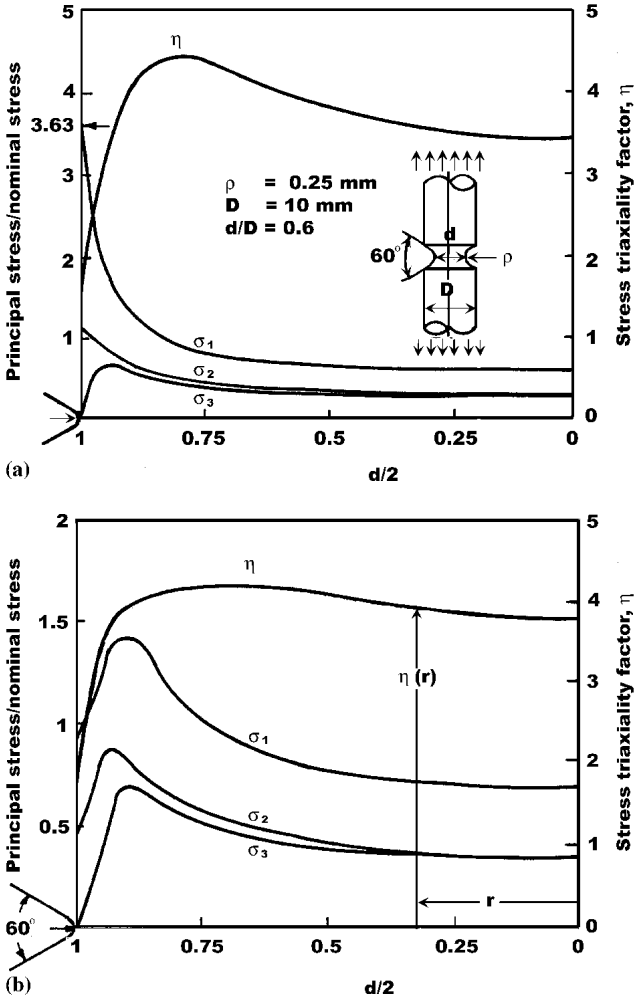

Fig. 7 Finite element results of the variation of the stress components and of the stress triaxiality factor across the notched tensile specimen for ρ = 0.25 mm, assuming: **(a)** an elastic material state, and **(b)** an elastic-plastic material state

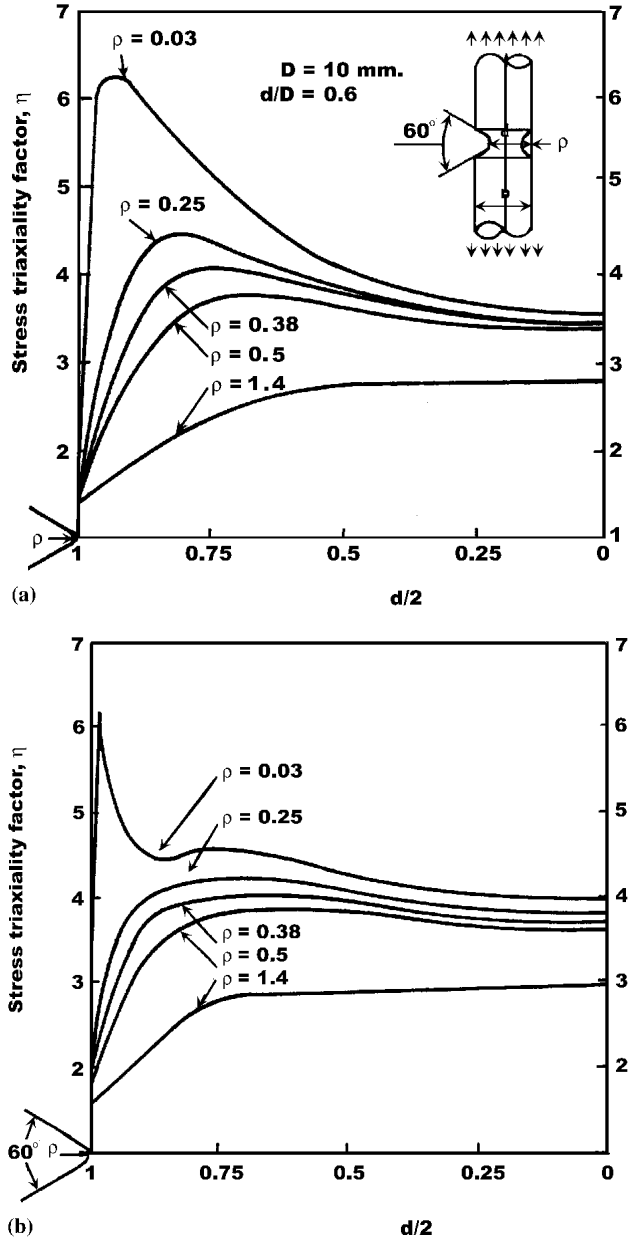

Fig. 8 Finite element results of the variation of the stress triaxiality factor, η, across the notched tensile specimen for five notch radii, assuming: **(a)** an elastic material state, and **(b)** an elastic-plastic material state

Table 4 summarizes the FE computation of the elastic stress concentration factor (K_t) and the average triaxiality factor ($\overline{\eta}$) across the notched section from both elastic and elastic-plastic FE analyses. Further, the table lists the theoretical K_t values obtained from the Neuber method.[12] The FE computed values of K_t deviate from the theoretical values by no more than −2%, which indicates the reasonable accuracy of the present FE analysis.

Figure 9 depicts the variation of $\overline{\eta}$ and K_t with ρ. Beyond the notch radius value of 0.25 mm, the values of $\overline{\eta}$ in the elastic-plastic material state are slightly higher than the corresponding values in the elastic state. On the other hand, the value of $\overline{\eta}$ in the elastic state for ρ = 0.03 mm is slightly higher than its value in the elastic-plastic state. In the current study, the higher value of $\overline{\eta}$ in the two material states is adopted. Thus, the computed values of $\overline{\eta}$ are 4.94, 3.95, 3.68, 3.50, and 2.57 for ρ = 0.03, 0.25, 0.38, 0.5, and 1.4 mm, respectively.

3.3 Predicted Versus Experimental NSR Values

A model developed by Majima et al.[3] has been used to predict NSR for the six steel grades of notch geometries shown in Fig. 1. The model predicts the NSR of the notched specimens for low-strength steels as follows:

$$\mathrm{NSR} = 0.6\left(\frac{\delta_L}{\delta_T}\right)^{0.5} \cdot (\overline{\eta} - 1)^{0.39} + 1 \qquad \text{(Eq 4)}$$

Using the FE computation of $\overline{\eta}$ (Table 4) of the current study and Eq 4, the predicted NSR curve of the notched test specimens for each steel grade is also shown in Fig. 3. For ρ ≥ 0.38 mm, the predictability of Eq 4 corresponds well with the experimental test results. However, the model of Majima et al. slightly devaluates NSR for material conditions A1, A2, and

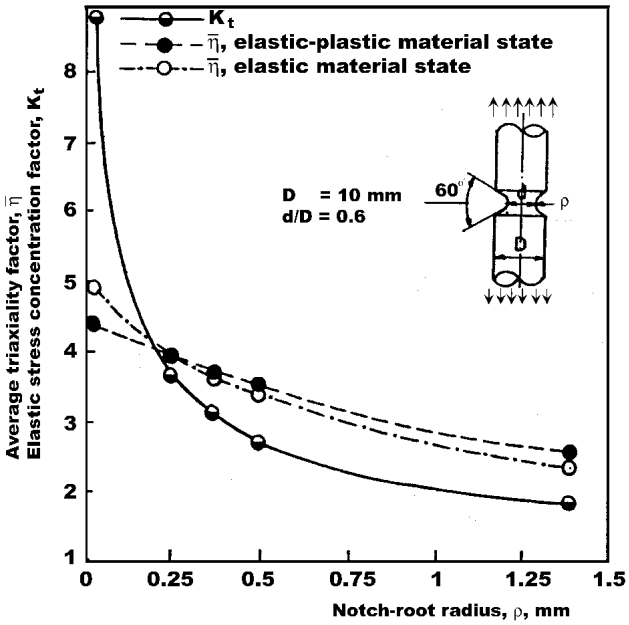

Fig. 9 Variations of the average triaxiality factor, $\bar{\eta}$, and the elastic stress concentration factor, K_t, with the notch-root radius, ρ

Table 4 Finite Element Computation of K_t and $\bar{\eta}$

Notch Radius, ρ, mm	Elastic Stress Concentration Factor, K_t		Average Triaxiality Factor, $\bar{\eta}$	
	Theoretical	Finite Element	Elastic	Elastic-Plastic
0.03	9.00	8.84	4.94	4.44
0.25	3.70	3.63	3.94	3.95
0.38	3.15	3.11	3.59	3.68
0.50	2.80	2.75	3.39	3.50
1.40	1.85	1.82	2.34	2.57

A3 of relatively medium hardness values, while it slightly overestimates NSR for material conditions A5 and A6 of higher hardness values. Thus, a factor, which is a function of material hardness, may be taken into consideration to improve the predictability of the model, for $\rho \geq 0.38$ mm, as follows.

Figure 10 depicts the variation of reduction of area in the notched specimens, RA_n, with ρ, for the six steel grades. The figure indicates that RA_n decreases with the increase of material hardness and the increase of notch sharpness (i.e., increase of $\bar{\eta}$). This can be expressed, for specified value of ρ, as:

$$[RA_n]\alpha[1/(\text{hardness} \cdot \bar{\eta})] \quad \text{(Eq 5a)}$$

Knowing from Table 2 that the reduction of area in smooth specimens (RA) decreases with the increase in material hardness, Eq 5a can be rewritten as:

$$[RA_n]\alpha[RA/\bar{\eta}] \quad \text{(Eq 5b)}$$

Figure 11 shows the variation of RA_n plotted versus $RA/\bar{\eta}$, which reasonably supports the validity of Eq 5b. Figure 3 indicates that $[NSR]\alpha[1/\rho]$, for $\rho \geq 0.38$ mm, while Fig. 9 depicts that $[\bar{\eta}]\alpha[1/\rho]$. Consequently, it can be concluded that $[NSR]\alpha[\bar{\eta}]$. Thus, Eq 5b can be rewritten as:

$$[RA_n \cdot NSR]\alpha[RA] \quad \text{(Eq 5c)}$$

At certain constant critical value of RA_n, Eq 5c indicates [NSR]α[RA]. Consequently, better predictability of NSR value is obtained by modifying the model of Majima et al. to take into account the effect of true ductility, $\varepsilon_f = \ln(100/(100 - RA\%))$, as follows:

$$NSR = 0.6\left(\frac{\delta_L}{\delta_T}\right)^{0.5} \cdot (\bar{\eta} - 1)^{0.39}[2\ln(2 + \varepsilon_f) - 1] + 1 \quad \text{(Eq 6)}$$

This expression is considered to be accurate within ± 4% for $\rho \geq 0.38$ mm. Figure 3 shows the excellent predictability of Eq 6, empirically derived in the current study and supported by FE computation of $\bar{\eta}$, compared with Eq 4 developed by Majima et al. The difference between the two models can be attributed to the fact that Majima et al. developed their model for the bluntly

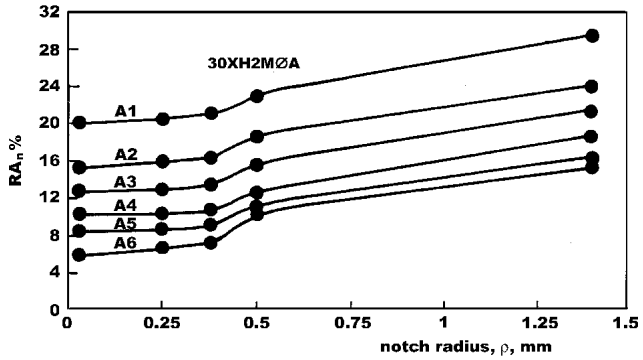

Fig. 10 Variation of the reduction of notched-net sectional area, RA_n, with the notch radius, ρ, for the six material grades

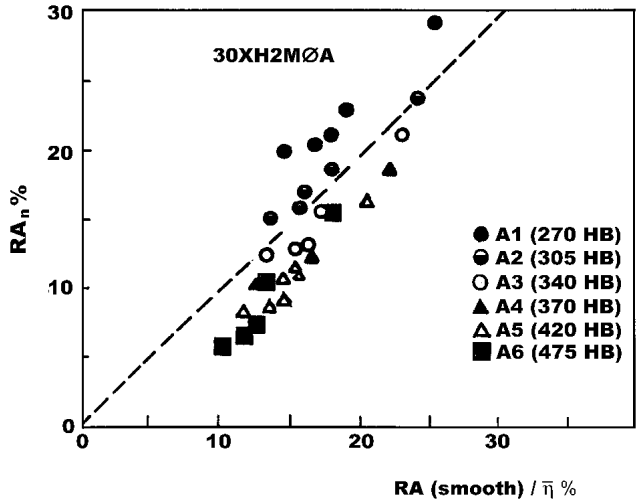

Fig. 11 Relation between the reduction of notched-net-sectional area, RA_n, and the ratio of reduction of area in smooth specimen to average triaxiality factor, $RA/\bar{\eta}$

U-shaped notch of d/D = 0.6 and ρ = 1, 2, 3 mm. Further, they approximated the value of $\overline{\eta}$ with that of an infinitely deep hyperbolic notch obtained by Neuber from the elastic stress distribution. Majima et al. approximated the value of $\overline{\eta}$ to be 3.93, 2.59, and 2.1, for ρ = 1, 2, and 3 mm, respectively. Comparing their value of $\overline{\eta}$ for the U-notch of d/D = 0.6 and ρ = 1 mm, $\overline{\eta}$ = 3.93 with the numerically determined value of $\overline{\eta}$ = 2.85 for the V-notch of the present work (Fig. 9) indicates that Majima et al. overestimated the value of $\overline{\eta}$ by 38%. Furthermore, Majima et al. conducted their investigation only on low-strength materials. However, in the range of ρ < 0.38 mm, the predictability of either Eq 4 or Eq 6 is unacceptable.

4. Conclusions

1) Six high strength martensitic steel grades, within hardness range of 270-475 HB, exhibited notch strengthening conditions employing V-notched specimens with: (a) outer diameter of 10 mm, (b) net-to-gross diameter ratio of 0.6, and (c) notch-root radius, ρ, range of 0.03-1.4 mm. Also, all the steel grades attained their maximum NSR values at ρ = 0.38 mm; thereafter, NSR decreases with the increase or decrease of ρ.
2) The notch tension test results have been used for successfully screening the plane strain fracture toughness behavior for the six high strength steel grades by extrapolating the corresponding ρ-NSR curves to ρ ≈ 0.0.
3) A model has been developed for more accurate prediction of NSR for the notched specimens of the six high-strength martensitic steel grades as a function of their uniaxial tensile properties and $\overline{\eta}$:

$$\mathrm{NSR} = 0.6\left(\frac{\delta_L}{\delta_T}\right)^{0.5} \cdot (\overline{\eta} - 1)^{0.39}[2\ln(2 + \varepsilon_f) - 1] + 1$$

This expression is considered to be accurate within ± 4% for ρ ≥ 0.38 mm.

Acknowledgments

A.M. Eleiche acknowledges the support of KFUPM in the preparation of the paper.

References

1. G.E. Dieter: *Mechanical Metallurgy*, McGraw-Hill, New York, 1988.
2. A.M. Agogino: "Notch Effects, Stress State, and Ductility," *J. Eng. Technol.*, 1978, *100*, pp. 348-55.
3. T. Majima, M. Anazai, and H. Makazawa: "Notch Tensile Strength of Ductile Materials," *Bull. JSME*, 1980, *29*, pp. 4000-04.
4. A.C. Mackenzie, J.W. Hancock, and D.K. Brown: "On the Influence of State of Stress on Ductile Failure Initiation in High Strength Steels," *Eng. Fract. Mech.*, 1977, *9*, pp. 167-88.
5. M.L. Fried and G. Sachs: "Notched Bar Tension Tests on Annealed Carbon Steel Specimens of Various Sizes and Contours" in *Symposium on Deformation of Metals as Related to Forming and Service*, *ASTM STP No. 87*, 1948, pp. 83-117.
6. E.A. Davis and F.M. Connelly: "Stress Distribution and Plastic Deformation in Rotating Cylinders of Strain Hardening Materials," *ASME J. Appl. Mech.*, 1959, *26*, pp. 25-30.
7. R.P. Reed, D.T. Read, and R.L. Tobler: "Notch Tensile Measurements and Fracture Toughness Correlations for Austenitic Stainless Steels" in *Advances in Cryogenic Engineering*, *3*, Plenum Press, New York, 1986, pp. 361-68.
8. N.M. Abd-Allah, M.S. El-Fadaly, M.M. Megahed, and A.M. Eleiche: "Fracture Toughness Properties of High Strength Martensitic Steel Within a Wide Hardness Range," *J. Mater. Eng. Performance,* 2001, *10*(5), pp. 576-85.
9. ASTM Standards: *Sharp-Notch Tension Testing With Cylindrical Specimens*, *E23*, ASTM International, West Conshohocken, PA, 1978.
10. ASTM Standards: *Standard Test Method for Plane-Strain Fracture Toughness of Metallic Materials*, *E399-90*, ASTM International, West Conshohocken, PA, 1994.
11. ASTM Standards: *Standard Test Method for J_{IC}, a Measure of Fracture Toughness*, *E813-89*, ASTM International, West Conshohocken, PA, 1991.
12. W.J. Harris: *Metallic Fatigue*, Pergamon Press, New York, 1962.